nanomanufacturing

MDPI

Article

Structure of the Charge-Transfer State in PM6/Y6 and PM6/Y6:YT Composites Studied by Electron Spin Echo Technique

Ekaterina A. Lukina [1], Aina V. Kulikova [1], Mikhail N. Uvarov [1], Alexander A. Popov [2], Ming Liu [3], Yong Zhang [3] and Leonid V. Kulik [1,*]

[1] Voevodsky Institute of Chemical Kinetics and Combustion of the Siberian Branch of the Russian Academy of Sciences, 630090 Novosibirsk, Russia
[2] Physical Department of Novosibirsk, State University, 630090 Novosibirsk, Russia
[3] School of Materials Science and Engineering, Harbin Institute of Technology, Harbin 150001, China; yongzhang@hit.edu.cn (Y.Z.)
* Correspondence: chemphy@kinetics.nsc.ru

Abstract: Nowadays, Y-shaped non-fullerene acceptors become increasingly important in organic photovoltaics (OPV). Their use in binary and ternary bulk heterojunction composites continuously pushes up the efficiency of OPV devices. However, the mechanism of OPV performance enhancement by the third component of a ternary composite is rarely understood. In the present work, pulse EPR technique was used to reveal the similarities and the differences of photoinduced charge separation process in binary PM6/Y6 and ternary PM6/Y6:Y-T composites, where PM6 is polymer donor, Y6 and Y-T are different non-fullerene acceptors. Out-of-phase electron spin echo signal was detected for both composites, which is the signature of the charge-transfer state (CT state) formed at the donor/acceptor interface upon exciton splitting. Nearly identical distribution of the distances between the electron and the hole constituting the CT state was obtained for these composites from the analysis of this signal. In both cases the average electron-hole distance was 3.5 nm. It implies that OPV efficiency increase with Y-T addition is not caused by the increased probability of CT state dissociation followed by free charge generation for PM6/Y6:Y-T composite.

Keywords: organic photovoltaics; semiconducting polymer; ternary composite; EPR; charge-transfer state

Citation: Lukina, E.A.; Kulikova, A.V.; Uvarov, M.N.; Popov, A.A.; Liu, M.; Zhang, Y.; Kulik, L.V. Structure of the Charge-Transfer State in PM6/Y6 and PM6/Y6:YT Composites Studied by Electron Spin Echo Technique. *Nanomanufacturing* **2023**, *3*, 123–134. https://doi.org/10.3390/nanomanufacturing3020008

Academic Editor: Andres Castellanos-Gomez

Received: 10 March 2023
Revised: 31 March 2023
Accepted: 3 April 2023
Published: 4 April 2023

1. Introduction

Sunlight is a clean and abundant source of energy that can be harvested for sustainable power generation, and is also the most important clean energy source on the Earth. Among the new-generation thin film solar cell technologies, organic solar cells (OSCs) based on environmentally friendly organic photovoltaic materials have attracted a lot of attention [1–3]. The OSCs have the advantages of being low-cost, light-weight, flexible, semi-transparent and solution-processable with roll-to-roll or slot-die methods [4], while the currently widespread inorganic solar cells based on silicon are heavy, opaque and aesthetically unappealing. The high fabrication cost of silicon solar panels and the environment problem during fabrication also restrict their use.

OSCs are generally composed on the active layer which is responsible for charge photogeneration, and the electron-selective and the hole-selective layers, which facilitate directional charge transport from the active layer into the electrodes—the cathode and the anode. Typically, a bulk-heterojunction (BHJ) composite of electron donor (usually conjugated polymer) and acceptor (for example, n-type molecular semiconductor) materials with nanoscale morphology is used as the active layer. The first BHJ OSC was reported in 1995 by Heeger et al. [5]. At early stage, the researchers in this field were mostly focusing on the development of polymer donors and understanding their blends with the fullerene

acceptors, mainly $PC_{60}BM$ and $PC_{70}BM$. However, the drawbacks of fullerene derivatives limited the further advances on the power conversion efficiencies (PCEs). Replacement of the ubiquitous fullerene acceptors with novel non-fullerene acceptors (NFAs) over the past few years have led to the rapid improvement in the performance of OSCs with PCEs beyond 18% for single junction cells [6].

The photoelectric conversion process of OSC includes three main processes: first, the light absorption and exciton generation in the active layer; second, the excitons separation process; and third, the charge carrier transport and collection [7]. After the active layer absorbs light, an electronically excited state of the donor or the acceptor molecule (the exciton) is formed. The exciton then undergoes a rapid charge transfer (CT) process, which produces an interfacial CT state, also known as a geminate radical pair (RP) or bound polaron pair at the interface between the donor phase and the acceptor phase. The free carriers (electron and holes) that are produced after charge separation migrate in the acceptor and donor phases, respectively, and finally are collected by the electrodes or lost via recombination, either geminate or non-geminate. The charge separation at the interface is an important process that affects the short-circuit current (I_{sc}) of solar cells, and also has some influence on the open circuit voltage (V_{oc}) of OSCs. The photophysical processes in the active layer are mainly affected by the order of its blending and are closely related to the interface that is formed by the donor and acceptor. Therefore, this means that the study of the abovementioned light-induced physical processes needs to be combined with characterization of the properties of the donor and the acceptors (such as, miscibility, crystallinity and aggregation, etc.). Furthermore, an in-depth understanding of this light-induced physical process will also be able to point out the direction and new ideas for the molecular design of the active layer material. However, little research has been done on the kinetics of charge separation in the active layer, which is due to the lack of related techniques and the complexity of the interaction between the donor and the acceptor in the active layer. Transient absorption spectroscopy is currently a common method in studying the kinetic process of charge separation in the active layer, but it can only provide a macroscopic-level understanding due to its overlapping signal peaks of ground and excited state species in donor and acceptor phases. Experimental study of the CT state—the principal intermediate of the photoelectric conversion in OSCs—is difficult because it is transient and usually short-living, and therefore cannot be generated at high concentration. For this reason, the optical signals of the CT state (either absorption or luminescence) are typically weak. In addition, they overlap with corresponding signals from other species in donor/acceptor composite. In favorable cases optical methods provide some information about the spectral and lifetime of the CT state [8–10]. However, these methods are generally not able to extract the information about the geometrical structure of the CT state.

The method of choice to study the structure of the CT state is Electron Paramagnetic Resonance (EPR) spectroscopy. EPR is a magnetic resonance technique based on the interaction of the magnetic moment of the unpaired electron spin with the external magnetic field. As mentioned above, the active layer of the OSC after photoexcitation produces a positive and the negative polaron [11]. Both polarons carry the unpaired electron spin, and from a chemistry viewpoint they are ion-radicals. Since EPR is sensitive only to paramagnetic species, it probes the photogenerated charges selectively. Typically, they are captured at the energy traps which come from the structural disorder in the donor/acceptor blend. Therefore, the light-induced EPR signal is directly related to the molecular structure of the donor and acceptor and their aggregation behavior, and the degree of structural disorder in the blend film. Continuous wave (CW) light-induced EPR can be used to study the non-geminate (bulk) recombination of the photogenerated charges in organic photovoltaic (OPV) composites [11–13]. Time-resolved (TR) EPR can be used to probe the CT state in donor–acceptor composites [14–16]. However, TR EPR spectroscopy also experiences the major problem of the difficulty of signal assignment. Electron spin echo (ESE, also known as pulse EPR), in particular, in its out-of-phase ESE (OOP ESE) version can be more informative and selective, since the signal is formed due

to the correlation of the spins of positive and negative polarons constituting CT state [17]. The CT state is created upon the exciton splitting on (sub)picosecond timescale [18,19] followed by subsequent thermalization of the electron and the hole, which typically requires several nanoseconds [20,21]. Since this process is fast, the correlation between the electron spins of the electron and the hole constituting the CT state is preserved. It is important that the exciton, as the precursor of the CT state (has a definite electron spin, usually zero (singlet exciton) [22,23], although triplet excitons (spin $S = 1$) can contribute to charge photogeneration in special cases [24]. The principal reason for the appearance of the OOP ESE is the mutual correlation of the spins of the electron and the hole within the CT state. Previously, OOP ESE was successfully used for determining the length of initial photoinduced electron transfer in bacterial photosynthetic reaction centers (RCs) and plant photosystems [25,26] and also in model donor–acceptor compounds [27]. For donor–acceptor systems with well-defined geometry this spectroscopy allows the measurement of the distance between the positive and the negative charges within the geminate pair (another name for the CT state) with angstrom precision [28,29].

The conventional architecture of OSC implies the use of the two-component donor–acceptor composite as the active layer of a solar cell. Nevertheless, it limits the feasible efficiency of this device mostly because the of relatively narrow spectral range for solar light absorption. One can use more complex architectures, such as tandem cells [30] or ternary cells [31], to overcome this limitation. Both these architectures allow the enhancement of efficiency by about the same extent. Tandem solar cells are hard to produce in a large scale; besides, they are quite unstable. This makes ternary cells, which are more stable and simple, and therefore more promising. Active medium of a ternary cells consists of three different organic compounds. Such cells composed using conjugated polymers as the donor and fullerene-derivative or non-fullerene molecules as the acceptors have been already characterized by several research groups. Even though the variety of ternary systems reveals a high efficiency factor of over 18%, the photovoltaic conversion mechanism behind them, in particular, the mechanism of primary charge separation, is not understood as well as it is for binary systems. Electron spin echo spectroscopy offers an attractive possibility to reveal the features of the CT state structure and dynamics for ternary OPV composites with two fullerene acceptors [32] and one fullerene and one non-fullerene acceptor [13]. In the present work, ESE spectroscopy is applied for the first time for ternary OPV blend with two non-fullerene acceptors Y6 and Y-T, which are the narrow band-gap and wide band-gap NFAs, respectively. For the ternary composite PM6/Y6:Y-T the same structure of the CT state as in the binary composite PM6/Y6 was found. This implies the mechanism of OPV performance improvement by the third component other than cascade electron transfer, previously identified for another highly efficient ternary OPV composite PBDB-T/PC_{70}BM:ITIC [13].

2. Materials and Methods

Y-T was synthesized according to Yin et al. [33] PM6 and Y6 was purchased from Solarmer Inc. (Beijing, China), with 99.9% purity. The chemical structures of these molecules are shown in Figure 1. To prepare the EPR samples, chlorobenzene solutions of PM6 with either Y6 or Y-T at 1:1 donor/acceptor weight ratio and a total concentration of 20 mg/mL were prepared. To prepare the ternary BHJ blend, the solution containing PM6, Y6 and Y-T with 1:0.85:0.15 weight ratio and a total concentration of 20 mg/mL was used. This proportion of the compounds corresponds to the optimum composition of the ternary blend which produced the best OPV performance [33]. The solutions were put in the quartz EPR tube of 4.5 mm outer diameter. During the evaporation of the chlorobenzene in a vacuum of about 10^{-3} Pa, the tube was sonicated in an ultrasonic bath. This caused the deposition of the homogeneous donor/acceptor composite on the inner wall of the EPR sample tube. The composites were annealed at 150 °C for 10 min in a vacuum of about 10^{-3} Pa. The estimated thickness of the composite film was about 500 nm, which was calculated on the basis of the substance weight, its density and the film area.

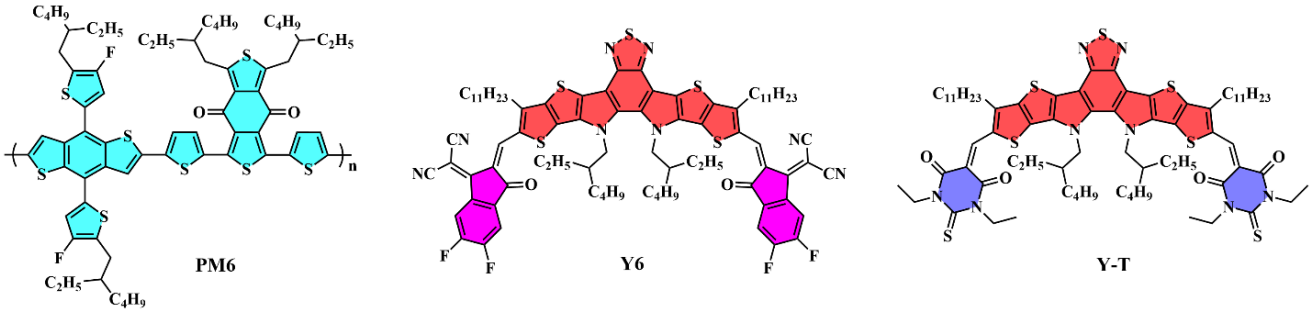

Figure 1. Chemical structures of the compounds used for preparing the composites (electron donor: PM6, electron acceptors: Y6 and Y-T).

Additionally, PM6/Y6 composite was prepared by spin-coating at 2000 rpm from the abovementioned chlorobenzene solution on a glass coverslip with thickness of 0.25 mm. This resulted in the formation of thin PM6/Y6 composite film with the thickness of about 100 nm. The coverslip with PM6/Y6 film was then cut to pieces and placed inside glass EPR sample tube with 4.95 mm outer diameter and heated for 150 °C during 10 min in a vacuum of about 10^{-3} Pa.

X-band EPR spectrometer ELEXSYS ESP-580E was used for electron spin echo experiments. Dielectric resonator ER 4118 X-MD-5 was mounted inside the cryostat (Oxford Instruments CF 935). Cold nitrogen gas flow was used to stabilize the temperature at 80 K. As usual, the phase of the in-phase ESE signal was adjusted by the dark ESE signal of the species in thermal equilibrium. In OOP ESE experiments the sample inside the resonator was excited by the laser flashes generated by TECH-laser (Laser-export Co. Ltd., Russia). This laser produced flashes with a duration of 5 ns, wavelength of 527 nm and a pulse repetition rate of 1 kHz. About 15 μJ of the light energy per flash was absorbed by the sample. The light was delivered to the sample through the quartz light-guide which was mounted inside the sample holder. ESE signal was induced by a two-pulse microwave sequence, *Flash–DAF*-π/4–τ–π–τ–*echo*. Here, *DAF* stands for Delay After laser Flash, and the π-pulse had nominal duration 24 nanoseconds. Such a pulse sequence is optimal for detecting the out-of-phase ESE signal of spin-correlated pairs. Note that the first pulse had nominal magnetization turning angle of π/4, in contrast to commonly used π/2-pulse [25]. The whole ESE signal in tome domain was integrated with the gate of 240 ns centered at the echo maximum. An additional π/2-pulse was applied 3 μs before the laser pulse with the aim to saturate the ESE signal of the (meta)stable radicals. This is necessary for measuring the relatively weak ESE signal of the CT state without distortion. Generally, the procedure of the experiment was close to that in our previous studies of OPV composites by pulse EPR technique [12,34].

3. Results

To investigate the short-living paramagnetic photoinduced species, which are typical intermediates of photoelectric conversion in OPV devices, pulse EPR experiments with laser excitation of donor/acceptor composites were performed. The contribution to the observed ESE signal from long-living paramagnetic species (stable defect state and metastable photoaccumulated charges in deep energetic traps) was suppressed by the pre-saturating microwave pulse. This procedure allows to observe the ESE signal generated solely by the laser pulse immediately preceding the echo-forming microwave pulse sequence [34]. As can be seen in Figure 2, in-phase echo-detected EPR spectra are very similar for PM6/Y6 and PM6/Y6:Y-T composites. They demonstrate a relatively strong absorptive (positive) line at the high-field part of the spectrum and a weak broad line at the low-field part. The emission/absorption spectral patterns are often observed in echo-detected EPR experiments on organic photovoltaic composites at low temperatures and small DAF values. This was observed for composites of donor polymer with different acceptors: fullerene [17]; non-fullerene small molecule [12]; and semiconducting carbon nanotubes [35]. Such a pattern is

generated in the course of spin evolution of the CT state accompanying its thermalization in the constant magnetic field of the EPR spectrometer, during which the spins of the charges constituting the CT state acquire the opposite polarization [16,36,37].

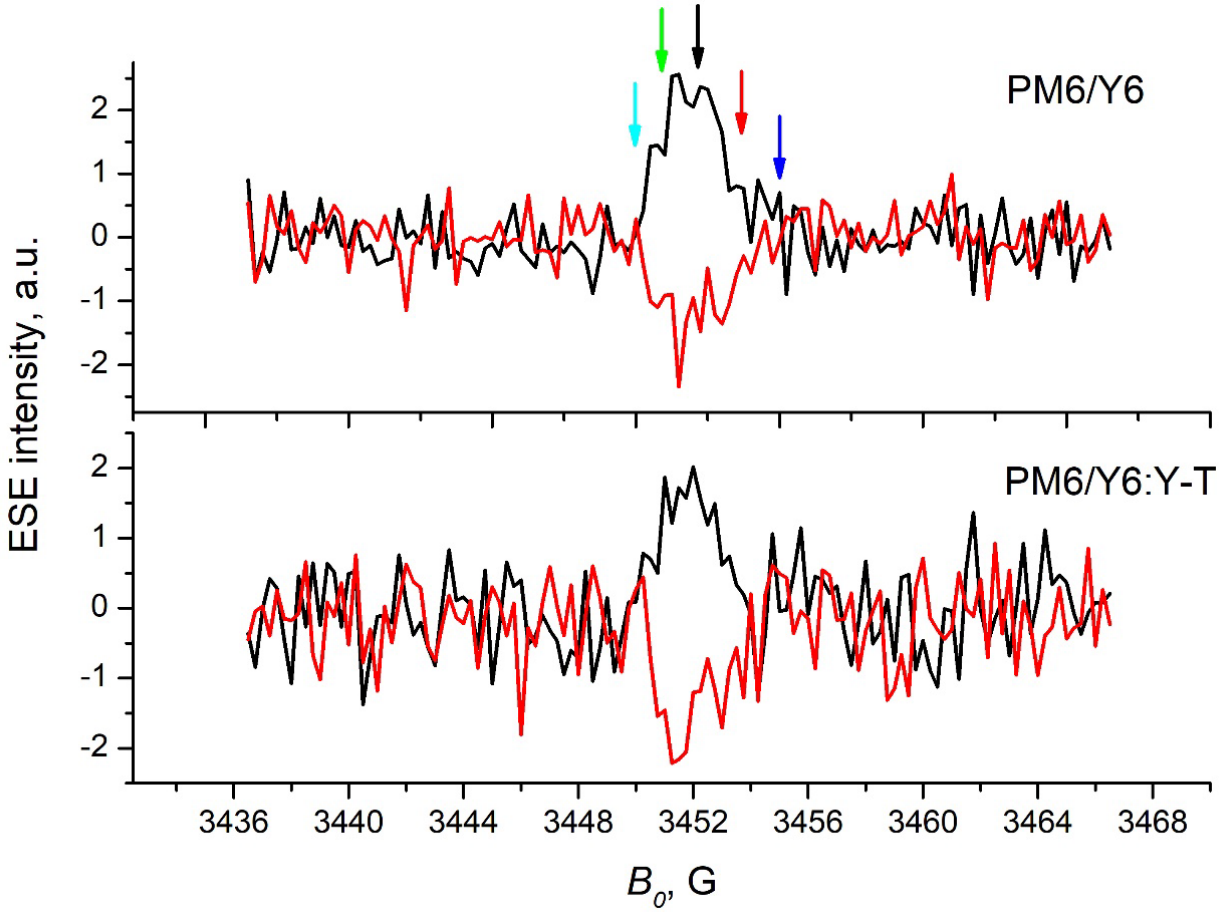

Figure 2. Echo-detected EPR spectra of the spin-polarized species in PM6/Y6 (upper panel) and PM6/Y6:Y-T (lower panel) composites on the walls of the sample tube taken at temperature 80 K with DAF = 1 μs. Black lines correspond to in-phase component of the spectra; red lines correspond to out-of-phase component of the spectra. Colored arrows mark the magnetic field positions used for the averaging of ESEEM traces.

The out-of-phase component of the echo-detected EPR spectra were also very similar for PM6/Y6 and PM6/Y6:Y-T composites (see Figure 2). For both composites, the spectrum was a relatively narrow single line. Due to the small width of the EPR line out-of-phase ESE decay trace became dependent on the spectral position (magnetic field value at which ESE decay was recorded, see Figure 3). This complicates the analysis of the dipolar modulation in the out-of-phase ESE. To avoid this complication, ESE decay traces were averaged over magnetic field position. According to the theoretical framework, this averaging suppresses artifacts in out-of-phase ESE decay caused by inhomogeneous microwave excitation of the EPR spectrum and restores pure dipolar modulation of the out-of-phase ESE [38]. The dependence of such field-averaged OOP ESE intensity $M_x(\tau)$ on the interval τ between two echo-forming microwave pulses is determined by interspin distance distribution function $G(R)$:

$$M_x(\tau) = \exp(-[2\tau/T_2]^{\delta}) \int G(R) \iint \sin[\omega_d(R,\theta,\phi)\tau] \sin(\theta) d\theta d\varphi dR, \quad (1)$$

where T_2 is the transversal relaxation time for electron spins (stretched exponential decay of the transversal magnetization decay the exponent δ is assumed here instead of monoex-

ponential decay), R is the distance between the centers of spin density distributions of the electron and the hole, θ and φ are polar and azimuthal angles, respectively, for the vector of the external magnetic field B_0 in the reference frame of the principal axes of Zero-Field Splitting (ZFS) tensor. ZFS tensor, in turn, is determined by the magnetic dipolar interaction between the spins of the electron and the hole within the CT state. The dipolar frequency ω_d is determined by ZFS parameters D and E:

$$\omega_d = 2\pi[\frac{2D(R)}{3}\left(1 - 3\cos^2\theta\right) + 2E(R)\sin^2\theta\cos 2\varphi]. \quad (2)$$

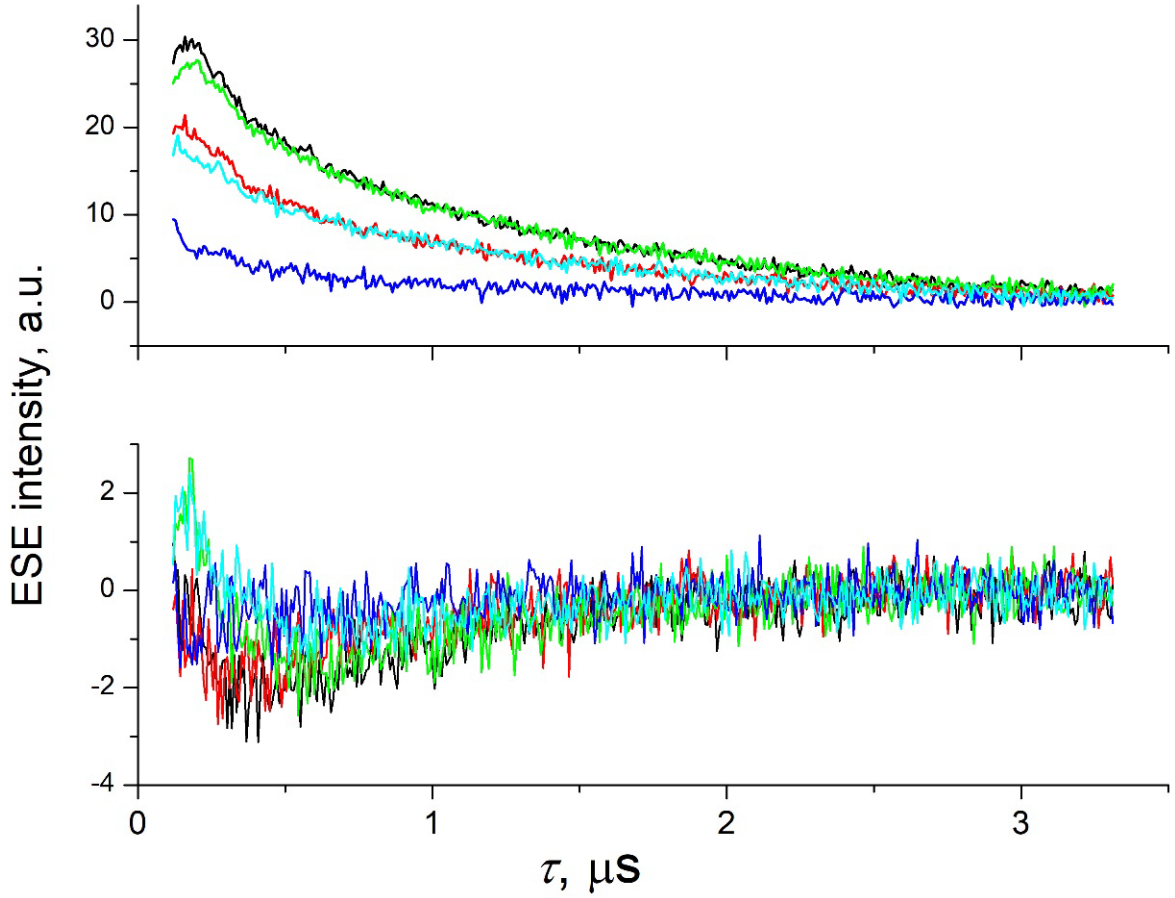

Figure 3. In-phase (upper panel) and out-of-phase (lower panel) ESEEM traces for PM6/Y6 composite taken at different magnetic field at 80 K with DAF = 1 μs. The color code corresponds to the color of the arrows in Figure 2. For in-phase ESE experiment the pre-saturating microwave pulse was switched off.

For point-dipoles approximation $E(R) = 0$ and $D(R) = 3/2\ \gamma^2/(\hbar R^3)$, where γ is free electron gyromagnetic ratio and $\hbar$ is the Planck constant. In the present work we used more realistic parametrization of $E(R)$ and $D(R)$, obtained by quantum chemical calculation of the CT state at P3HT/PC_{60}BM interphase [38]. Although different donors and acceptors were used in the present study and in Lukina et al. [38] this parametrization qualitatively reproduces hole delocalization over the donor polymer. We note that for PM6/Y-T composite the intensity of out-of-phase ESE signal in analogous experiment is much smaller than that for PM6/Y6 and PM6/Y6:Y-T composites (Figure S1 in Supporting Information). This points to low yield of light-induced charge separation in PM6/Y-T composite and is in general agreement with its much lower OPV efficiency compared to that of PM6/Y6 and PM6/Y6:Y-T composites [33].

Field-averaged two-pulse in-phase ESE decay for PM6/Y6 composite is shown in Figure 4. As can be seen, it can be reasonably approximated by stretched exponential decay with effective T_2 = 1320 ns and δ = 0.7. These values are used further for simulation of out-of-phase ESE traces. The deviation of ESE decay from monoexponential function is typical for solid samples. For BHJ composites it is probably caused by spatial and energetic disorder at the donor/acceptor interphase [34].

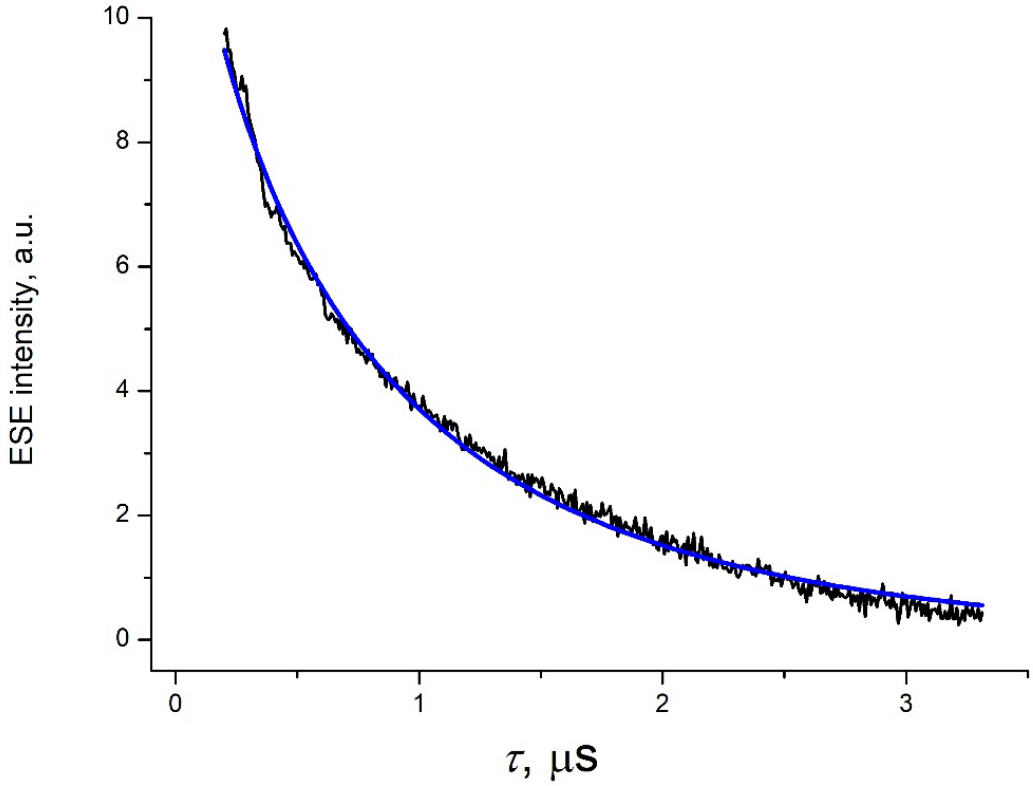

Figure 4. Field-averaged in-phase ESEEM trace for PM6/Y6 composite (black line) taken at 80 K with DAF = 1 μs and its simulation with stretched exponential decay function (blue line). The pre-saturating microwave pulse was switched off.

As can be seen from Figure 5, out-of-phase ESEEM traces for PM6/Y6 and PM6/Y6:Y-T composites are also very similar. Consequently, numerical modeling of these traces according to Equation (2) yields nearly identical interspin distance distribution density functions (see Figure 6). The modeling was based on Tikhonov regularization. It was performed using a procedure similar to that used recently to model the CT state structure in binary and ternary OPV composites of donor polymer PBDB-T, fullerene acceptor $PC_{70}BM$ and non-fullerene acceptor ITIC [13].

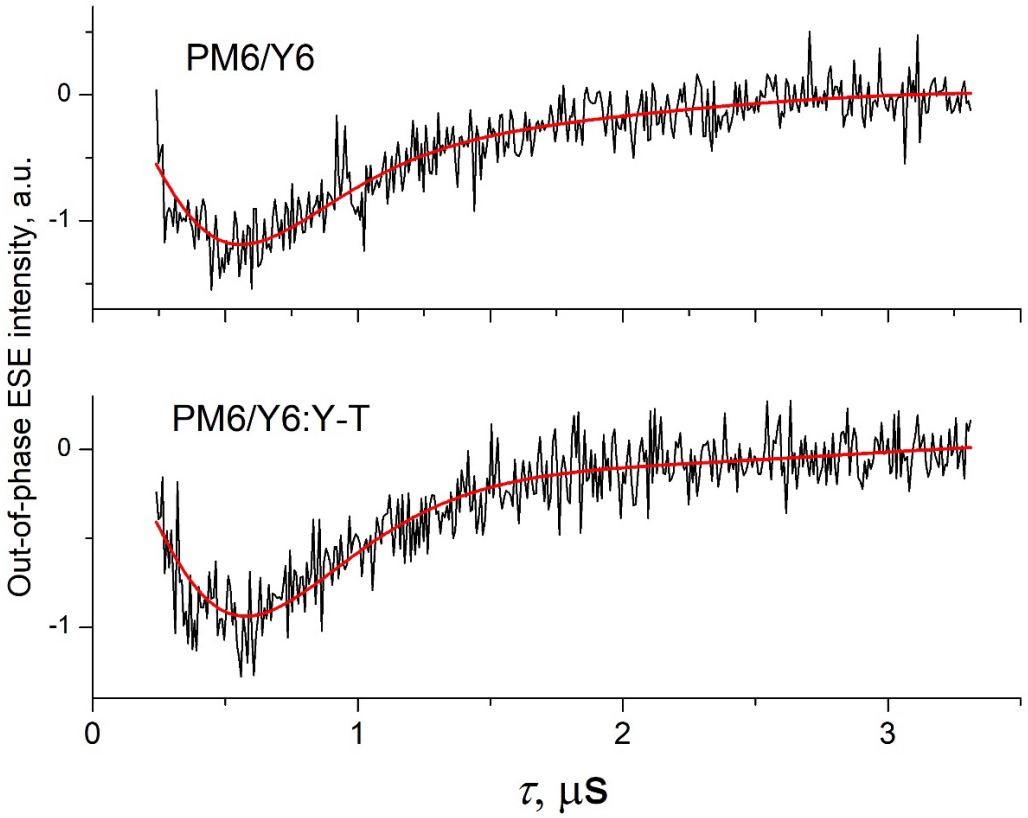

Figure 5. Field-averaged out-of-phase ESEEM trace for PM6/Y6 (upper panel) and PM6/Y6:Y-T (lower panel) composites taken at a temperature of 80 K with DAF = 1 μs (black lines) and their numerical simulations according to Equation (2) (red lines).

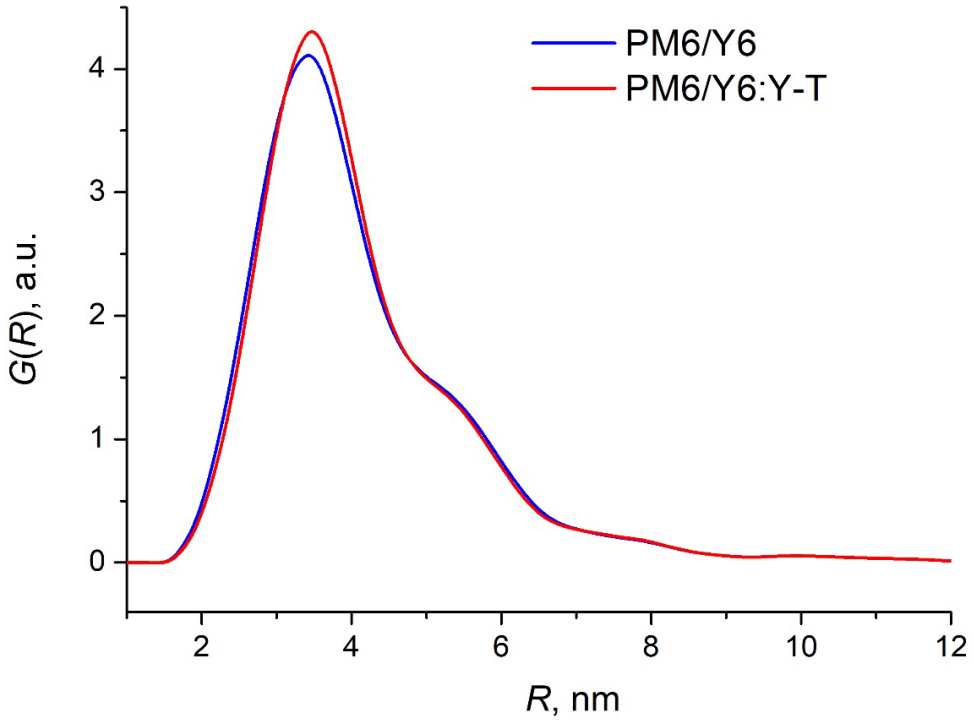

Figure 6. The interspin distance distribution density for the charge-transfer state in PM6/Y6 (blue line) and PM6/Y6:Y-T (red line) composites obtained from numerical simulation of the out-of-phase ESEEM traces at Figure 3.

4. Discussion

With a good degree of accuracy, the interspin distance between the components of the CT state equal to electron-hole distance. Thus, as can be derived from Figure 6, the maximum electron-hole distance distribution density for the CT state in PM6/Y6 composite occurs at R = 3.5 nm. For PM6/Y6:Y-T composite this maximum occurs at nearly the same distance R = 3.6 nm. Both these values are close to the corresponding value for PBDB-T/PC_{70}BM:ITIC composite [13], which demonstrated high efficiency of charge photogeneration [39,40]. It is evident that for PM6/Y6 and PM6/Y6:Y-T composites the average electron-hole distance within the CT state is sufficiently long to provide very high yield of free charge generation, which is close to unity [41]. This is in contrast to PBDB-T/PC_{70}BM:ITIC composite, in which cascade electron transfer between the fullerene and the non-fullerene acceptors leads to an increase in the average electron-hole distance within the CT state for the ternary composites compared to that for binary ones [13]. This leads to higher yield of the CT state separation for the ternary composite PBDB-T/PC_{70}BM:ITIC compared to that of the corresponding binary ones. The inefficiency of cascade electron transfer in PM6/Y6:Y-T composite can be caused by the similarity of chemical structure of the acceptors, Y6 and Y-T. This similarity promotes their intimate mixing, in contrast to pronounced phase segregation of the acceptors of different structure, PC_{70}BM and ITIC, in PBDB-T/PC_{70}BM:ITIC composite. Another possible reason for inefficiency of cascade electron transfer in PM6/Y6:Y-T composite is related to the order of HOMO and LUMO energy levels in this system. Since LUMO energies of PM6 and Y-T are nearly the same, while that of Y6 is noticeably lower [33], exciton generation at PM6 preferably leads to electron transfer from PM6 to Y6, without engaging Y-T. Similarly, since HOMO energies of PM6, Y6 and Y-T are also close, with the HOMO energy of Y-T being the highest in this series, exciton generation at Y-T does not lead to efficient hole transfer to Y6 (which would enable the cascade hole transfer further to PM6) or directly to PM6. Thus, the most probable process responsible for "ternary gain" in PM6/Y6:Y-T composite is sensibilized charge transfer enabled by Y-T, proposed by Yin et al. [33]. This process implies photon absorption by Y-T, whose optical absorption spectrum fills the gap between absorption bands of PM6 and Y6. The absorption spectrum of Y6 strongly overlaps with the luminescence spectrum of Y-T, which ensures efficient energy transfer from Y-T to Y6, with further hole transfer from PM6 to Y6.

Finally, we note that the field-averaged out-of-phase ESEEM trace for PM6/Y6 composite spin-coated on glass plate (Figure S2 in Supporting Information) has the same shape as ESEEM trace for PM6/Y6 composite cast on the walls of the EPR tube (Figure 5) accumulated at otherwise identical conditions. This confirms that the method of the composite preparation does not have a decisive influence on the structure of the CT state. This is reasonable, since the structure of the CT state is governed by local morphology of the donor/acceptor interface, which in turn is determined by the molecular structure of the donor and the acceptor. This observation is in line with a similar observation for another NFA-based OPV composite [12].

5. Conclusions

Electron spin echo spectroscopy revealed the very similar structure of the charge-transfer state for highly efficient OPV composites PM6/Y6 and PM6/Y6:Y-T. This implies the existence of the same mechanism of the charge separation at the donor/acceptor interface for the binary PM6/Y6 composite and the ternary PM6/Y6:Y-T composite. This also allows us to confirm the assignment of "ternary OPV gain" mechanism (the positive influence of small quantity of Y-T introduced to PM6/Y6 system) to energy transfer from photoexcited Y-T to Y6, enabling sensibilized charge transfer between PM6 and Y6. Overall, the present results demonstrate the potential of pulse EPR spectroscopy, in combination with other spectroscopic methods, for elucidating the mechanism of photoelectric conversion in complex OPV systems.

Supplementary Materials: The following supporting information can be downloaded at: https://www.mdpi.com/article/10.3390/nanomanufacturing3020008/s1, Figure S1: Echo-detected EPR spectrum of the spin-polarized species in PM6/Y-T composite; Figure S2: Field-averaged out-of-phase ESEEM trace for PM6/Y6 composite spin-coated on glass plate.

Author Contributions: Conceptualization, Y.Z. and L.V.K.; methodology, L.V.K.; software, A.A.P.; validation, E.A.L. and M.N.U.; formal analysis, E.A.L.; investigation E.A.L. and A.V.K.; resources, M.L. and Y.Z.; writing—original draft preparation, L.V.K.; writing—review and editing, Y.Z. and L.V.K.; visualization, M.N.U.; funding acquisition, Y.Z. and L.V.K. All authors have read and agreed to the published version of the manuscript.

Funding: The work was funded in accordance with the state assignment of V.V. Voevodsky Institute of Chemical Kinetics and Combustion of the Siberian Branch of the Russian Academy of Sciences (No. AAAA-A21-121011390038-1). Y. Zhang thanks the support from the National Key Research and Development Program of China (2021YFE0105800).

Data Availability Statement: The data presented in this study are available on request from the corresponding author.

Conflicts of Interest: The authors declare no conflict of interest.

References

1. Zhu, L.; Zhang, M.; Xu, J.; Li, C.; Yan, J.; Zhou, G.; Zhong, W.; Hao, T.; Song, J.; Xue, X.; et al. Single-Junction Organic Solar Cells with over 19% Efficiency Enabled by a Refined Double-Fibril Network Morphology. *Nat. Mater.* **2022**, *21*, 656–663. [CrossRef]
2. Gao, W.; Qi, F.; Peng, Z.; Lin, F.R.; Jiang, K.; Zhong, C.; Kaminsky, W.; Guan, Z.; Lee, C.; Marks, T.J.; et al. Achieving 19% Power Conversion Efficiency in Planar-Mixed Heterojunction Organic Solar Cells Using a Pseudosymmetric Electron Acceptor. *Adv. Mater.* **2022**, *34*, 2202089. [CrossRef] [PubMed]
3. Tamai, Y. Charge Generation in Organic Solar Cells: Journey toward 20% Power Conversion Efficiency: Special Issue: Emerging Investigators. *Aggregate* **2022**, *3*, e280. [CrossRef]
4. Jee, M.H.; Ryu, H.S.; Lee, D.; Lee, W.; Woo, H.Y. Recent Advances in Nonfullerene Acceptor-Based Layer-by-Layer Organic Solar Cells Using a Solution Process. *Adv. Sci.* **2022**, *9*, 2201876. [CrossRef]
5. Yu, G.; Gao, J.; Hummelen, J.C.; Wudl, F.; Heeger, A.J. Polymer Photovoltaic Cells: Enhanced Efficiencies via a Network of Internal Donor-Acceptor Heterojunctions. *Science* **1995**, *270*, 1789–1791. [CrossRef]
6. Liu, Q.; Jiang, Y.; Jin, K.; Qin, J.; Xu, J.; Li, W.; Xiong, J.; Liu, J.; Xiao, Z.; Sun, K.; et al. 18% Efficiency Organic Solar Cells. *Sci. Bull.* **2020**, *65*, 272–275. [CrossRef]
7. Deibel, C.; Strobel, T.; Dyakonov, V. Role of the Charge Transfer State in Organic Donor-Acceptor Solar Cells. *Adv. Mater.* **2010**, *22*, 4097–4111. [CrossRef]
8. Barker, A.J.; Chen, K.; Hodgkiss, J.M. Distance Distributions of Photogenerated Charge Pairs in Organic Photovoltaic Cells. *J. Am. Chem. Soc.* **2014**, *136*, 12018–12026. [CrossRef]
9. Dong, Y.; Cha, H.; Bristow, H.L.; Lee, J.; Kumar, A.; Tuladhar, P.S.; McCulloch, I.; Bakulin, A.A.; Durrant, J.R. Correlating Charge-Transfer State Lifetimes with Material Energetics in Polymer: Non-Fullerene Acceptor Organic Solar Cells. *J. Am. Chem. Soc.* **2021**, *143*, 7599–7603. [CrossRef] [PubMed]
10. Azzouzi, M.; Gallop, N.P.; Eisner, F.; Yan, J.; Zheng, X.; Cha, H.; He, Q.; Fei, Z.; Heeney, M.; Bakulin, A.A.; et al. Reconciling Models of Interfacial State Kinetics and Device Performance in Organic Solar Cells: Impact of the Energy Offsets on the Power Conversion Efficiency. *Energy Environ. Sci.* **2022**, *15*, 1256–1270. [CrossRef]
11. Lukina, E.A.; Uvarov, M.N.; Kulik, L.V. Charge Recombination in P3HT/$PC_{70}BM$ Composite Studied by Light-Induced EPR. *J. Phys. Chem. C* **2014**, *118*, 18307–18314. [CrossRef]
12. Kobeleva, E.S.; Popov, A.A.; Baranov, D.S.; Uvarov, M.N.; Nevostruev, D.A.; Degtyarenko, K.M.; Gadirov, R.M.; Sukhikh, A.S.; Kulik, L.V. Origin of Poor Photovoltaic Performance of Bis(Tetracyanoantrathiophene) Non-Fullerene Acceptor. *Chem. Phys.* **2021**, *546*, 111162. [CrossRef]
13. Popov, A.A.; Uvarov, M.N.; Kulik, L.V. Mode of Action of the Third Component in Ternary Organic Photovoltaic Blend PBDB-T/ITIC: PC70BM Revealed by EPR Spectroscopy. *Synth. Met.* **2021**, *277*, 116783. [CrossRef]
14. Behrends, J.; Sperlich, A.; Schnegg, A.; Biskup, T.; Teutloff, C.; Lips, K.; Dyakonov, V.; Bittl, R. Direct Detection of Photoinduced Charge Transfer Complexes in Polymer Fullerene Blends. *Phys. Rev. B* **2012**, *85*, 125206. [CrossRef]
15. Kobori, Y.; Noji, R.; Tsuganezawa, S. Initial Molecular Photocurrent: Nanostructure and Motion of Weakly Bound Charge-Separated State in Organic Photovoltaic Interface. *J. Phys. Chem. C* **2013**, *117*, 1589–1599. [CrossRef]
16. Niklas, J.; Poluektov, O.G. Charge Transfer Processes in OPV Materials as Revealed by EPR Spectroscopy. *Adv. Energy Mater.* **2017**, *7*, 1602226. [CrossRef]

17. Lukina, E.A.; Popov, A.A.; Uvarov, M.N.; Kulik, L.V. Out-of-Phase Electron Spin Echo Studies of Light-Induced Charge-Transfer States in P3HT/PCBM Composite. *J. Phys. Chem. B* **2015**, *119*, 13543–13548. [CrossRef] [PubMed]
18. Piris, J.; Dykstra, T.E.; Bakulin, A.A.; van Loosdrecht, P.H.M.; Knulst, W.; Trinh, M.T.; Schins, J.M.; Siebbeles, L.D.A. Photogeneration and Ultrafast Dynamics of Excitons and Charges in P3HT/PCBM Blends. *J. Phys. Chem. C* **2009**, *113*, 14500–14506. [CrossRef]
19. Dong, Y.; Cha, H.; Zhang, J.; Pastor, E.; Tuladhar, P.S.; McCulloch, I.; Durrant, J.R.; Bakulin, A.A. The Binding Energy and Dynamics of Charge-Transfer States in Organic Photovoltaics with Low Driving Force for Charge Separation. *J. Chem. Phys.* **2019**, *150*, 104704. [CrossRef]
20. Van der Kaap, N.J.; Koster, L.J.A. Charge Carrier Thermalization in Organic Diodes. *Sci. Rep.* **2016**, *6*, 19794. [CrossRef] [PubMed]
21. Melianas, A.; Etzold, F.; Savenije, T.J.; Laquai, F.; Inganäs, O.; Kemerink, M. Photo-Generated Carriers Lose Energy during Extraction from Polymer-Fullerene Solar Cells. *Nat. Commun.* **2015**, *6*, 8778. [CrossRef] [PubMed]
22. Niklas, J.; Beaupré, S.; Leclerc, M.; Xu, T.; Yu, L.; Sperlich, A.; Dyakonov, V.; Poluektov, O.G. Photoinduced Dynamics of Charge Separation: From Photosynthesis to Polymer–Fullerene Bulk Heterojunctions. *J. Phys. Chem. B* **2015**, *119*, 7407–7416. [CrossRef] [PubMed]
23. Lukina, E.A.; Suturina, E.; Reijerse, E.; Lubitz, W.; Kulik, L.V. Spin Dynamics of Light-Induced Charge Separation in Composites of Semiconducting Polymers and $PC_{60}BM$ Revealed Using Q-Band Pulse EPR. *Phys. Chem. Chem. Phys.* **2017**, *19*, 22141–22152. [CrossRef] [PubMed]
24. Lukina, E.A.; Reijerse, E.; Lubitz, W.; Kulik, L.V. Spin-Dependent Recombination of the Charge-Transfer State in Photovoltaic Polymer/Fullerene Blends. *Mol. Phys.* **2019**, *117*, 2654–2663. [CrossRef]
25. Dzuba, S.A.; Gast, P.; Hoff, A.J. ESEEM Study of Spin-Spin Interactions in Spin-Polarised P^+QA^- Pairs in the Photosynthetic Purple Bacterium *Rhodobacter Sphaeroides* R26. *Chem. Phys. Lett.* **1995**, *236*, 595–602. [CrossRef]
26. Zech, S.G.; van der Est, A.J.; Bittl, R. Measurement of Cofactor Distances between $P_{700}^{\bullet+}$ and $A_1^{\bullet-}$ in Native and Quinone-Substituted Photosystem I Using Pulsed Electron Paramagnetic Resonance Spectroscopy. *Biochemistry* **1997**, *36*, 9774–9779. [CrossRef] [PubMed]
27. Carmieli, R.; Mi, Q.; Ricks, A.B.; Giacobbe, E.M.; Mickley, S.M.; Wasielewski, M.R. Direct Measurement of Photoinduced Charge Separation Distances in Donor–Acceptor Systems for Artificial Photosynthesis Using OOP-ESEEM. *J. Am. Chem. Soc.* **2009**, *131*, 8372–8373. [CrossRef] [PubMed]
28. Hoff, A.J.; Gast, P.; Dzuba, S.A.; Timmel, C.R.; Fursman, C.E.; Hore, P.J. The Nuts and Bolts of Distance Determination and Zero- and Double-Quantum Coherence in Photoinduced Radical Pairs. *Spectrochim. Acta Part A Mol. Biomol. Spectrosc.* **1998**, *54*, 2283–2293. [CrossRef]
29. Al Said, T.; Weber, S.; Schleicher, E. OOP-ESEEM Spectroscopy: Accuracies of Distances of Spin-Correlated Radical Pairs in Biomolecules. *Front. Mol. Biosci.* **2022**, *9*, 890826. [CrossRef] [PubMed]
30. Zheng, Z.; Wang, J.; Bi, P.; Ren, J.; Wang, Y.; Yang, Y.; Liu, X.; Zhang, S.; Hou, J. Tandem Organic Solar Cell with 20.2% Efficiency. *Joule* **2022**, *6*, 171–184. [CrossRef]
31. Günther, M.; Kazerouni, N.; Blätte, D.; Perea, J.D.; Thompson, B.C.; Ameri, T. Models and Mechanisms of Ternary Organic Solar Cells. *Nat. Rev. Mater.* **2023**. [CrossRef]
32. Kulik, L.V.; Uvarov, M.N. Charge Photogeneration and Recombination in Ternary Organic Photovoltaic Blend PCDTBT/PC60BM/ICBA Studied by EPR Spectroscopy. *Appl. Magn. Reson.* **2020**, *51*, 1071–1078. [CrossRef]
33. Yin, Y.; Zhan, L.; Liu, M.; Yang, C.; Guo, F.; Liu, Y.; Gao, S.; Zhao, L.; Chen, H.; Zhang, Y. Boosting Photovoltaic Performance of Ternary Organic Solar Cells by Integrating a Multi-Functional Guest Acceptor. *Nano Energy* **2021**, *90*, 106538. [CrossRef]
34. Beletskaya, E.A.; Lukina, E.A.; Uvarov, M.N.; Popov, A.A.; Kulik, L.V. Geminate Recombination in Organic Photovoltaic Blend PCDTBT/PC_{71} BM Studied by out-of-Phase Electron Spin Echo Spectroscopy. *J. Chem. Phys.* **2020**, *152*, 044706. [CrossRef]
35. Uvarov, M.N.; Kobeleva, E.S.; Degtyarenko, K.M.; Zinovyev, V.A.; Popov, A.A.; Mostovich, E.A.; Kulik, L.V. Fast Recombination of Charge-Transfer State in Organic Photovoltaic Composite of P3HT and Semiconducting Carbon Nanotubes Is the Reason for Its Poor Photovoltaic Performance. *Int. J. Mol. Sci.* **2023**, *24*, 4098. [CrossRef]
36. Hore, P.J. RESEARCH NOTE Transfer of Spin Correlation between Radical Pairs in the Initial Steps of Photosynthetic Energy Conversion. *Mol. Phys.* **1996**, *89*, 1195–1202. [CrossRef]
37. Popov, A.A.; Lukina, E.A.; Rapatskiy, L.; Kulik, L.V. Time-Domain Shape of Electron Spin Echo Signal of Spin-Correlated Radical Pairs in Polymer/Fullerene Blends. *J. Magn. Reson.* **2017**, *276*, 86–94. [CrossRef]
38. Lukina, E.A.; Popov, A.A.; Uvarov, M.N.; Suturina, E.A.; Reijerse, E.J.; Kulik, L.V. Light-Induced Charge Separation in a P3HT/PC_{70} BM Composite as Studied by out-of-Phase Electron Spin Echo Spectroscopy. *Phys. Chem. Chem. Phys.* **2016**, *18*, 28585–28593. [CrossRef]
39. Wang, B.; Fu, Y.; Yan, C.; Zhang, R.; Yang, Q.; Han, Y.; Xie, Z. Insight Into the Role of PC71BM on Enhancing the Photovoltaic Performance of Ternary Organic Solar Cells. *Front. Chem.* **2018**, *6*, 198. [CrossRef]

40. Li, Q.; Sun, Y.; Xue, X.; Yue, S.; Liu, K.; Azam, M.; Yang, C.; Wang, Z.; Tan, F.; Chen, Y. Insights into Charge Separation and Transport in Ternary Polymer Solar Cells. *ACS Appl. Mater. Interfaces* **2019**, *11*, 3299–3307. [CrossRef]
41. Perdigón-Toro, L.; Zhang, H.; Markina, A.; Yuan, J.; Hosseini, S.M.; Wolff, C.M.; Zuo, G.; Stolterfoht, M.; Zou, Y.; Gao, F.; et al. Barrierless Free Charge Generation in the High-Performance PM6: Y6 Bulk Heterojunction Non-Fullerene Solar Cell. *Adv. Mater.* **2020**, *32*, 1906763. [CrossRef] [PubMed]